3-D Full-Loop Simulation of an Industrial-Scale Circulating Fluidized-Bed Boiler

Bona Lu, Nan Zhang, Wei Wang, and Jinghai Li
State Key Laboratory of Multiphase Complex Systems, Institute of Process Engineering, Chinese Academy of Sciences, Beijing, 100190, P.R. China

John H. Chiu and Shin G. Kang
ALSTOM Power, Inc., 2000 Day Hill Road, Windsor, CT 06095

DOI 10.1002/aic.13917
Published online October 18, 2012 in Wiley Online Library (wileyonlinelibrary.com).

Three-dimensional (3-D) simulations using an Eulerian multiphase model were employed to explore flow behaviors in a full-loop industrial-scale CFB boiler with and without fluidized-bed heat exchanger (FBHE), where three solids phases were employed to roughly represent the polydisperse behavior of particles. First, a simulation of the boiler without FBHE is implemented to evaluate drag models, in terms of pressure profiles, mixing behaviors, radial velocity profiles, etc. Compared to the conventional model, the simulation using the energy-minimization multiscale (EMMS) model successfully predicts the pressure profile of the furnace. Then, such method is used to simulate the boiler with FBHE. The simulation shows that solid inventory in the furnace is underpredicted and reduced with an increase of the valve opening, probably due to the underevaluated drag for FBHE flows. It is suggested to improve EMMS model which is now based on a single set of operating parameters to match with the full-loop system.
© 2012 American Institute of Chemical Engineers *AIChE J,* 59: 1108–1117, 2013
Keywords: full-loop simulation, multiscale, boiler, drag model, polydisperse particles

Introduction

During the past 30 years, circulating fluidized bed (CFB) combustion has been developed into a mainstream technology. To achieve successful design of CFB combustor with high efficiency and low emissions, scale-up experiencing trials at the bench, pilot, demonstration, and commercial scale is very costly. Therefore, the application of modern simulation tools, like computational fluid dynamics (CFD), can be of vital importance to the scale-up of CFB boilers.

In general, two different approaches might be used for the simulation of gas–solid flows in CFB systems, namely the Lagrangian or the Eulerian approach. Comparatively, the Eulerian approach is more acceptable for industry applications because of the advantage in computation expense.[1] The publications about CFB modeling in a Eulerian way may be further subdivided into those that only consider the hydrodynamic behavior, and the others that also investigate the combustion phenomena. A very good predication of the combustion process relies on a reasonable flow model. However, many early relevant simulations are based on the simplified or empirical flow model due to immature numerical techniques or limited computational resources.[2–4] Recently, there are some attempts to analyze the steady or dynamic combustion behaviors based on a comprehensive flow model with a simultaneous solution of the conservation equations of each phase of fluid flow.[5–6] However, most of those simulations are restrained to the single furnace or chamber. Zhang et al.[7–8] first reported the 3-D full-loop simulation of a large-scale CFB boiler, and pointed out that the full-loop simulation has an advantage over the simulation of only one part of CFB boiler, since much detailed information in terms of, for example, the dynamic mixing of gas and solid fuels both horizontally and vertically, the effects of various nonuniform geometries, especially the pressure balance over the whole loop of CFB circulation can be obtained. Such a formidable task requires high-computation recourses. It cannot be realized until. Recent research[9] found that the multiscale CFD approach (EMMS drag model is integrated into the Eulerian multiphase model) seems to reach a mesh-independent solution of the subgrid structure, and, thus, hopefully would realize a success in the full-loop simulation of an industrial-scale boiler using affordable computation resources.

The main goal of this study is to realize such simulations of a full-loop industrial-scale CFB boiler with and without FBHE and further probe into the hydrodynamic behaviors of gas and solid phase. The second goal is to seek suitable drag models for fitting for the full-loop system where multiple flow regimes usually coexist.

Numerical Description

Governing equations

The simulations were performed at the platform of FLUENT®6.3. The multiphase Eulerian granular model was used to study the flow behavior in the boiler. The drag coefficient was reported to be affected significantly by inhomogeneous structures and hence had the dominant role in simulation predictions.[10–15] Therefore, two different drag coefficients with and without considering the particle clustering, i.e.,

Correspondence concerning this article should be addressed to B. Lu at bnlu@home.ipe.ac.cn.

© 2012 American Institute of Chemical Engineers

Table 1. Formulas of H_D for the CFB Boiler (ρ_p = 2598.4 kg/m^3, ρ_g = 0.315 kg/m^3, μ_g = 4.55e-5 Pa·s, $\bar{d}_p$ = 129.74 μm, U_g = 7.236 m/s, G_s = 39.2 kg/(m^2 s), ε_{mf} = 0.4, ε_{max} = 0.9997)

Formulae ($H_D = a(Re_s+b)^c$, $0.001 \le Re_s \le 1000$)	Range ($\varepsilon_{mf} \le \varepsilon_g \le 1$)
$\begin{cases} a = 0.12621 + 0.51327\exp\left(-0.5\left(\frac{\varepsilon_g - 0.51738}{0.05325}\right)^2\right) \\ c = 0 \end{cases}$	$0.4 < \varepsilon_g \le 0.51228$
$\begin{cases} a = 0.06022 + \frac{0.64769}{1+\left(\varepsilon_g/0.54069\right)^{38.95056}} \\ b = 1.26148 - \frac{1.25109}{\left(1+\exp\left(-(\varepsilon_g - 0.49842)/0.00835\right)\right)}\left(1 - \frac{1}{\left(1+\exp\left(-(\varepsilon_g - 0.68685)/0.03593\right)\right)}\right) \\ c = 0.27698 - \frac{0.298}{1+\left(\varepsilon_g/0.55363\right)^{29.78427}} \end{cases}$	$0.51228 < \varepsilon_g \le 0.60826$
$\begin{cases} a = 1/\left(15.09342 - 13.31486\varepsilon_g^{6.02771}\right) \\ b = -52.05197 + 346.18273\varepsilon_g - 914.53136\varepsilon_g^2 + 1202.33087\varepsilon_g^3 - 786.52213\varepsilon_g^4 + 204.82611\varepsilon_g^5 \\ c = 1/\left(3.51503 + 3.1596\varepsilon_g^{4.34314}\right) \end{cases}$	$0.60826 < \varepsilon_g \le 0.9904$
$\begin{cases} a = 0.52193 + \frac{0.8812}{1+\exp\left(-(\varepsilon_g - 0.99662)/0.00112\right)}\left(1 - \frac{1}{1+\exp\left(-(\varepsilon_g - 0.99752)/0.00006\right)}\right) \\ b = 0.47595 - \frac{0.22085}{1+\left(\varepsilon_g/0.99594\right)^{2170.31695}} \\ c = 0.13788 - 0.07951\exp\left(-0.5\left(\frac{\varepsilon_g - 0.99841}{0.00142}\right)^2\right) \end{cases}$	$0.9904 < \varepsilon_g < 0.9997$
$a = 1,\ c = 0$	$0.9997 \le \varepsilon_g \le 1$

EMMS-based model and Ergun/Wen and Yu, respectively, were evaluated in this study. It is worth noting that the non-uniform structures also influence the solid stress and viscosity.[13,16] However, compared to the interphase momentum transfer correlations, the effect of solid stress and viscosity models seems less important. Our previous simulation of a 2-D riser using the kinetic theory of granular flow (KTGF) revealed the similar results of Yang et al. using the empirical correlations of solids stress and visocity.[9,17] In this study, we use KTGF to describe solid-phase pressure and viscosity.

Drag model

Drag force plays an important role in simulation results. In the momentum transport equations, the drag force is represented by the term βu_{slip}, where, β is the interphase momentum exchange coefficient and has many correlations.

In this study, two correlations of drag coefficient were compared. One is a combination of the work of Ergun and Wen and Yu, which was given by Gidaspow.[18] The equations are written as follows

$$\begin{cases} \beta = \frac{3}{4}C_{D0}\frac{\varepsilon_s\varepsilon_g\rho_g\left|\boldsymbol{v}_g - \boldsymbol{v}_s\right|}{d_p}\varepsilon_g^{-2.65} & (\varepsilon_g \ge 0.8) \\ \beta = 150\frac{(1-\varepsilon_g)^2\mu_g}{\varepsilon_g d_p^2} + 1.75\frac{(1-\varepsilon_g)\rho_g\left|\boldsymbol{v}_g - \boldsymbol{v}_s\right|}{d_p} & (\varepsilon_g < 0.8) \end{cases} \quad (1)$$

with

$$\begin{cases} C_{D0} = \frac{24\left(1+0.15Re_s^{0.687}\right)}{Re_s} & \text{for } Re_s < 1000. \\ C_{D0} = 0.44 & \text{for } Re_s \ge 1000 \end{cases} \quad (2)$$

The other is obtained from EMMS-based model.[9] This EMMS-based model is simplified from the model of Wang and Li[19] and expressed by

$$\beta = \frac{3}{4}C_{D0}\frac{\varepsilon_s\varepsilon_g\rho_g\left|\boldsymbol{v}_g - \boldsymbol{v}_s\right|}{d_p}\varepsilon_g^{-2.65}H_D, \quad (3)$$

Where H_D is defined as β/β_0 (β_0: Wen and Yu) to account for the hydrodynamic disparity between homogeneous and heterogeneous fluidization. H_D is first calculated with EMMS model[9] and stored in a matrix. To facilitate its usage, before running simulation, it is regressed into a series of functions, as our previous work.[9,20] Table 1 summarizes the formulas of H_D under the operating conditions, which will be detailed later. It is worth noting that the operating parameters, i.e., U_g and G_s are based on the cross section of the upper furnace, and the particle dia. d_p is the mean diameter based on the size distribution of ash particles before simplification.

Geometry and mesh

The CFB boiler shown in Figure 1 was designed by ALSTOM, consisting of a two-stage furnace, a cyclone separator, a U-type valve and FBHE. The furnace is about 24.5 m high and 3.15 m I.D. for the lower furnace. The cross-sectional area of the upper furnace is 3.96 m × 3.96 m. This boiler was established in Chatham, New Brunswick, Canada. ALSTOM provided the operating conditions and experimental data. The relevant experiment procedure can refer to Couturier et al.[21,22]

Because solids inventory in FBHE is constant, first, a simplified geometry without FBHE as shown in Figure 1a is employed to evaluate drag models, where the gas flow from FBHE is compensated through the entry £4 to keep consistent with the original total gas flow rate. Second, the

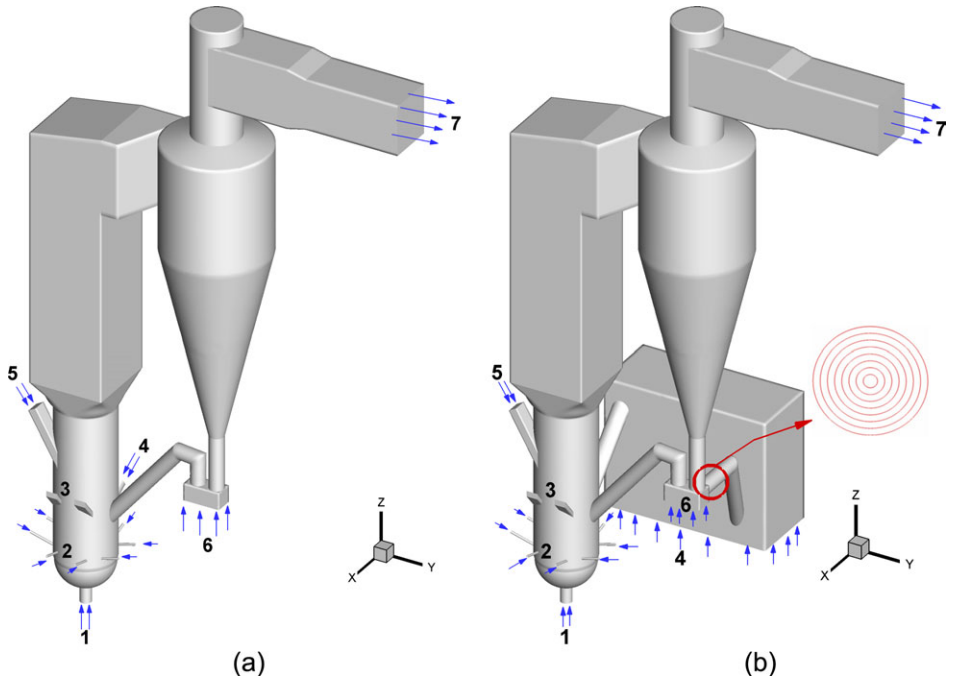

Figure 1. Schematic diagram of the 3-D reactors, 1- primary air inlet, 2-lower secondary air inlet, 3-fuel chute, 4-FBHE air, 5-upper secondary air inlet, 6-fluidized air for seal pot, and 7-pressure outlet.

(a) Geometry 1, neglecting FBHE, the corresponding air flow is compensated through the inlet £4, and (b) geometry 2, including FBHE, the red circle is the valve between the seal pot and FBHE. [Color figure can be viewed in the online issue, which is available at wileyonlinelibrary.com.]

Table 2. Physical Properties of Air and Particles

Air density ρ_g, kg/m^3		0.315	
Air viscosity μ_g, Pa·s		4.55×10^{-5}	
Particle density ρ_p, kg/m^3		2598	
		d_p	Mass ratio
Particle diameter d_p (μm) and mass ratio (%)	S1	646	6.73
	S2	117	92.66
	S3	24	0.61

more genuine geometry with FBHE shown in Figure 1b is simulated to explore the flow behavior as well as the influence of the opening of the valve between FBHE and the seal pot.

Gambit®2.4 is used to mesh the boiler. The hexahedral meshes are generated for most parts of the whole device, and tetrahedral meshes for the transition sections. The total grid number for geometries 1 and 2 is about 810,000 and 980,000, respectively.

Simulation settings

Figure 1 shows the geometries and the corresponding boundary settings. There is one primary air inlet, eight lower secondary air inlets (only two of them are open in this simulation), two fuel chutes, two fluidized air inlets, two upper secondary air inlets and one pressure outlet.

Fluent®6.3 is used as the solver, where an Eulerian multiphase model was employed. Table 2 shows the physical properties of gas phase and particles. The particles with a wide size distribution are divided into three groups to simulate the polydisperse behavior better. At the beginning, roughly 14,505.2 kg, 576.5 kg and 31,660 kg particles are packed in the furnace, seal pot and FBHE, respectively, and let the solids outflow recirculate into the furnace through the inlet 4 and inlet 3 for geometry 1 and geometry 2, respectively. If FBHE is not considered, the corresponding initial packed particles are also excluded. The gas flow rate for each inlet is presented in Table 3. More simulation settings are summarized in Table 4. The solids concentration in the furnace is continuously monitored. When it reaches the steady state, the process of time averaging is initiated. Generally, all cases are implemented for approximately 50 s in total, and latter 20 s are used for achieving the time-averaged data.

Table 3. Air Velocity for each Inlet

			Geometry 1		Geometry 2	
ID	Air inlet	Quantity	Air flow rate, kg/s	Solids con. ε_s	Air flow rate, kg/s	Solids con. ε_s
1	PA	1	9.321	0	9.321	0
2	LSA (south)	2	0.511	0	0.511	0
3	Fuel chute	2	0.511	0	0.511	0.3
4	Fluidized air	1	4.033	0.6	3.599	0
5	Upper sec. air	2	20.077	0	20.077	0
6	Air for seal pot	1	1.332	0	1.766	0
	Total		35.785		35.785	

Table 4. Simulation Settings in Fluent

Numbers of phases	4
Momentum & Volume discretization	First-order upwind
Drag coefficient (solid-solid)	Syamlal-obrien-symmetric
Drag coefficient (gas-solid)	Refer to section Drag model
Wall boundary	No-slip
Pressure outlet	1 atm
Granular temperature	Algebraic
Granular viscosity	Gidaspow
Granular bulk viscosity	Lun et al.
Frictional viscosity	Schaeffer
Frictional pressure	Based-ktgf
Angle of internal friction	30.00007
Solids pressure	Lun et al.
Radial distribution	Lun et al.
Restitution coefficient	0.9
Packing limit	0.7
Time step	5×10^{-4} s

Simulation of the Boiler without FBHE: Evaluation of Drag Models

Distribution of solids volume fraction and pressure

As mentioned previously, first, a simplified geometry is used for testing drag models. Figure 2 compares the transient distributions of solids volume fraction using both drag models. When the Ergun/Wen and Yu model is used, most particles are accumulated in the cyclone bottom while much less reside in the furnace. Comparatively, a larger number of particles are found to be nonuniformly distributed in the furnace when using EMMS-based model. Figure 3 illustrates the time-averaged pressure profile along the center line throughout the full-loop device, showing the difference between the distribution of solids inventory in the furnace and in the cyclone. The pressure drop for the cyclone is roughly more than three times that for the furnace when using Ergun/Wen and Yu model, while the pressure drop for both the cyclone and the furnace seems quite close if EMMS-based model is employed. To compare the pressure data with the experiment more directly, the calculated pressure profiles of the furnace using both models are delineated in Figure 4 where the measured values are indicated by the back dots. The comparison shows that EMMS-based model agrees well with the experiment at most elevations, while Ergun/Wen and Yu model only provides reasonable results above 2.5 m, but predicts much lower pressure at lower elevations. The pressure drop between elevations at 0 and 22.5 m using Ergun/Wen and

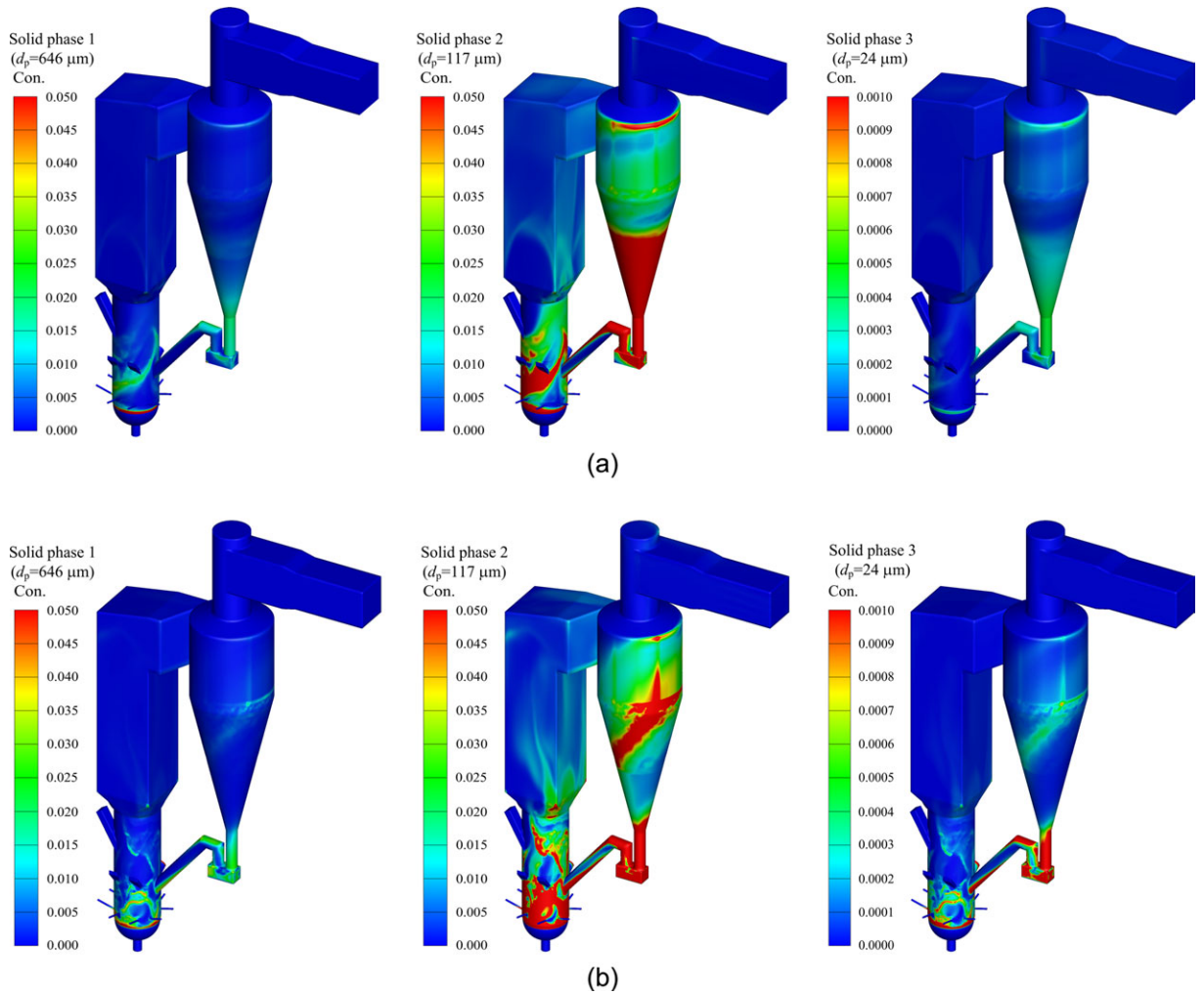

Figure 2. Snapshots of solids volume fraction (the solids concentration higher than 0.05 and 0.001 for solid phases 1 and 2, and solid phase 3, respectively, is also denoted in red color): (a) using Ergun/Wen and Yu model; (b) using EMMS-based model.

[Color figure can be viewed in the online issue, which is available at wileyonlinelibrary.com.]

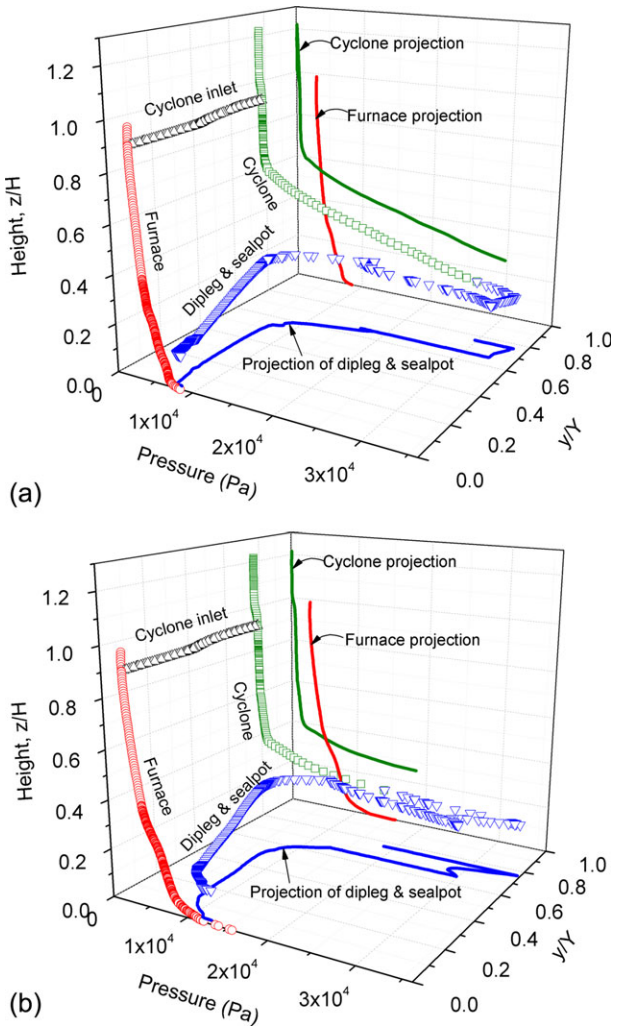

Figure 3. Simulated pressure balance in the full boiler ("0" in the *z*-direction is the position of the distributor above the plenum.

H is the total height of the furnace, *Y* is the distance between the centers of the furnace and the cyclone. The pressure data were obtained from the centerline of the furnace, cyclone inlet, cyclone, seal pot and dipleg): (a) using Ergun/Wen and Yu model; (b) using EMMS-based model. [Color figure can be viewed in the online issue, which is available at wileyonlinelibrary.com.]

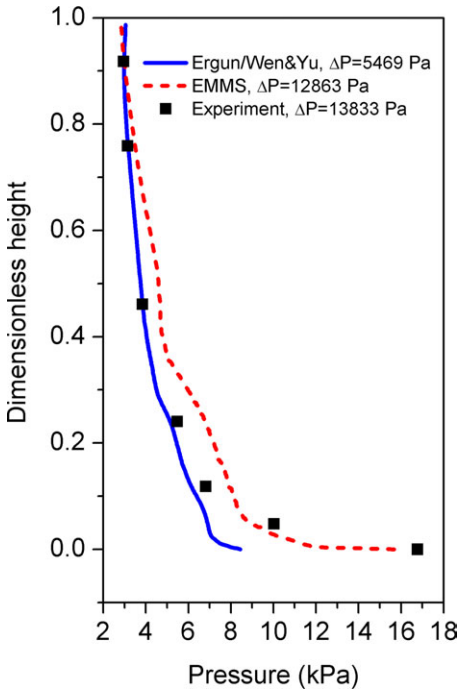

Figure 4. The comparison of the simulated axial profiles of pressure in the furnace and the experimental data.

[Color figure can be viewed in the online issue, which is available at wileyonlinelibrary.com.]

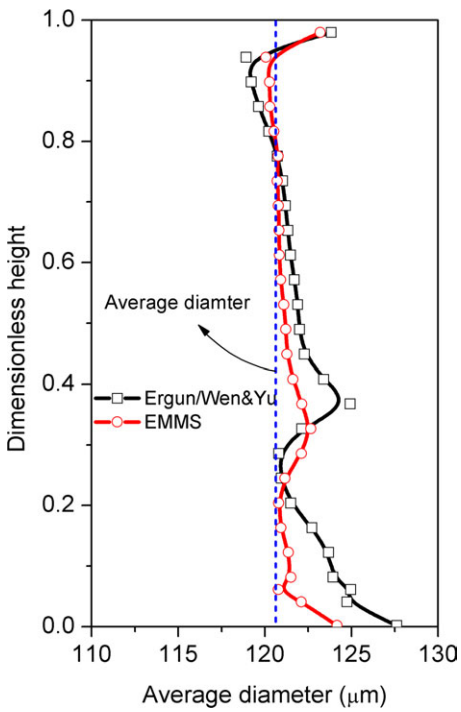

Figure 5. Axial profiles of cross-sectional average particle diameter $d_{ave,h}$ in the furnace (each position is scaled by the furnace height), $d_{ave,h}$ and d_{ave} (≈120.7 μm) represent the average particle diameter calculated from the size distribution of the entire granulate mixture at a given elevation and in the whole bed, respectively.

[Color figure can be viewed in the online issue, which is available at wileyonlinelibrary.com.]

Yu model (≈5,400 Pa) is nearly 39.5% of the experimental value (≈13,800 Pa).

Mixing behavior of three solid phases

Average particle diameter is often used to characterize the mixing behavior to some extent.[23–24] Figure 5 illustrates the variation of cross-sectional average particle dia. $d_{ave,h}$ along the furnace height, where $d_{ave,h}$ and d_{ave} represent the average particle diameter calculated from the size distribution of the entire granulate mixture at a given elevation and in the whole bed, respectively. Thus, when $d_{ave,h}$ is much closer to d_{ave}, the bed is mixed better. Since the solid phase with the smallest diameter (S3) accounts for a very small percentage, this solid mixture can be considered to be nearly binary (S1 and S2). If $d_{ave,h}$ is greater than d_{ave}, the larger particles (S1) increases. Conversely, when $d_{ave,h}$ is less than d_{ave}, the smaller particles (S2) become more intense.

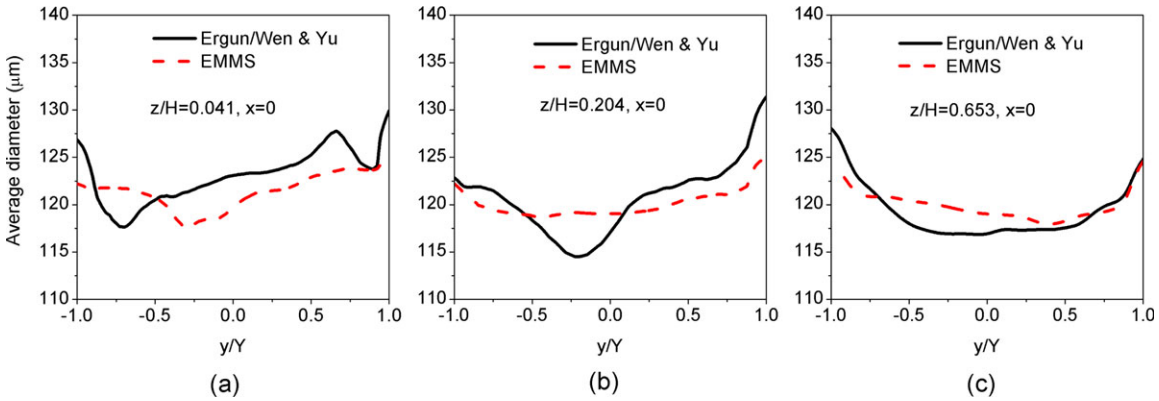

Figure 6. Radial profiles of average particle diameter at three elevations of the furnace (H is total height of the furnace, *Y* is the width of the furnace. *x* = 0): (a) z/H = 0.041; (b) z/H = 0.204, and (c) z/H = 0.653.

[Color figure can be viewed in the online issue, which is available at wileyonlinelibrary.com.]

Generally, as shown in Figure 5, the average particle diameter predicted by both models seems relatively smaller in upper furnace while larger at bottom. Compared to the total average dia. d_{ave}, the cross-sectional average particle dia. $d_{ave,h}$ at most elevations are larger, implying that larger particles (S1) tends to reside in the furnace while smaller particles (S2) are more readily blew away. For almost all the elevations, the cross-sectional average dia. $d_{ave,h}$ predicted by EMMS model is much closer to d_{ave} than Ergun/Wen and Yu model. This means that the simulation with EMMS model captures the better mixing behavior in the furnace. However, relevant experiment is not available to evaluate such mixing behavior of polydisperse particles.

Figure 6 delineates radial profiles of the average diameter at three heights. Larger diameters appear near the wall, especially at higher elevations, implying that larger particles are easier to fall down along the wall than the small particles. This tendency is not so obvious at the lower position, probably due to the influence of secondary air inlets and other supply entries.

Radial velocity profiles

Figure 7 compares the radial profiles of velocity of each phase using both drag models. It is clear to see that for both models, the velocity difference between gas and solid phase 1 are evident at all three elevations. When using Ergun/Wen and Yu model, the velocities of gas, solid phases 2 and 3

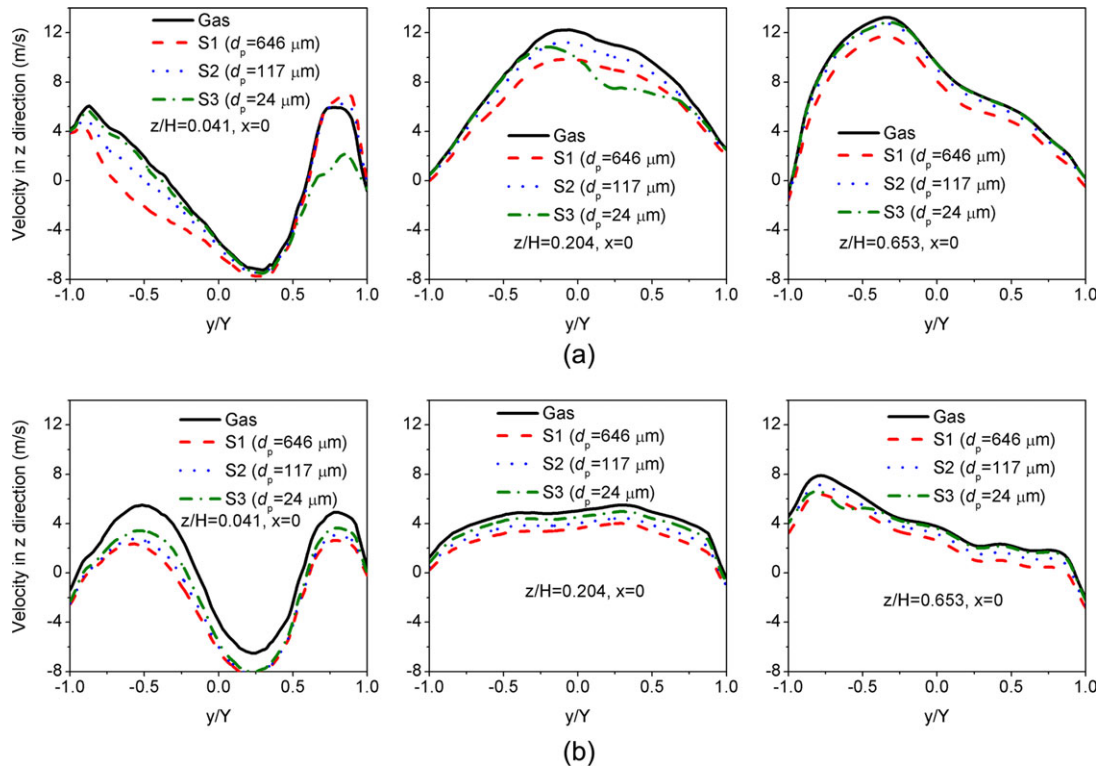

Figure 7. Radial profiles of the axial velocity of each phase at three elevations (H is the total height of the furnace, *Y* is the width of the furnace. *x* = 0): (a) using Ergun/Wen and Yu model; (b) using EMMS-based model.

[Color figure can be viewed in the online issue, which is available at wileyonlinelibrary.com.]

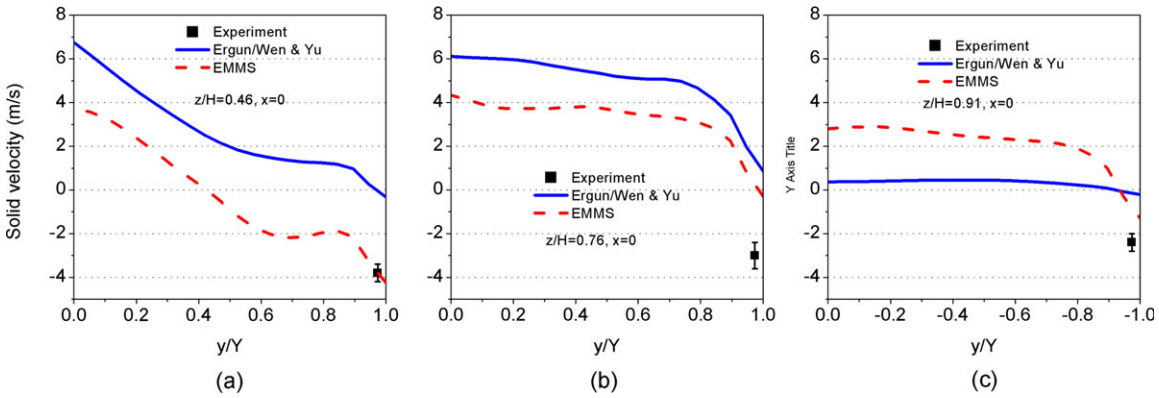

Figure 8. Comparison of calculated downward particle velocity near the wall and the measured values at three elevations (H is the total height of the furnace, *Y* is the width of the furnace.

***x* = 0): (a) z/H = 0.46; (b) z/H = 0.76, and (c) z/H = 0.91. [Color figure can be viewed in the online issue, which is available at wileyonlinelibrary.com.]**

almost overlap for each elevation. By comparison, such overlap only appears at the higher position (z/H = 0.653) when using EMMS-based model, implying that in the upper furnace exists an extremely dilute flow. In addition, large velocity differences between gas and other three solid phases can be observed clearly at the height of z/H = 0.041, suggesting the presence of particle clusters in the furnace bottom.

Downward particle velocity near the wall

Generally, stronger back mixing appears with larger downward particle velocity near the wall. Figure 8 compares the calculated particle velocity near the wall and the measured values. It can be found that the downward particle velocities near the wall provided by EMMS-based model are much larger than from Ergun/Wen and Yu model, showing more reasonable agreement with the experiment. We note that at the position of z/H = 0.76, the difference between simulated particle velocity near the wall and the measured downward velocity is bigger than at other two positions, and what is more, Ergun/Wen and Yu model predicts positive particle velocity near the wall. This position is just below the cyclone inlet, so we guess that the abrupt acceleration due to the shrinking mouth strongly disturbs the particle motion and also influences the measurement.

Solids flux

Figure 9 compares the calculated solids flux with the experimental data. The measured value is about 40 kg/(m^2 s). The simulated values are 47 kg/(m^2 s) and 55 kg/(m^2 s) for using Ergun/Wen and Yu model and EMMS-based model, respectively, a little higher than the measured data. This discrepancy is more probably induced by the simplification of particle-size distribution. Recent researches point out that particle polydispersity has an influence on solids stress[25–27] and also on the drag coefficient.[28] Therefore, it is necessary to account for the effect of polydisperisty in the computational fluid dynamic (CFD) simulation when the particles with a wide size distribution are involved.

Simulation of the boiler with FBHE: evaluation of valve opening ratio

For the boiler with FBHE, the opening ratio of the valve between the seal pot and FBHE is very critical. In practice, the opening of the value is often adjusted within a range due to the online operating situation. Therefore, the accurate value for the opening ratio is not easy to obtain. In the following simulations, two different opening ratios, i.e., 1.5625 and 25% (the smallest circle and the middle circle is open, respectively, refer to Figure1b), are chosen for investigating its impact on flow behaviors. For calculating gas–solid drag coefficient, EMMS-based model is used according to the above parametric study.

Distribution of solids volume fraction

Figure 10 shows the snapshots of solids volume fraction over the whole bed. It is clear to see that the solids volume fraction in FBHE increases significantly and simultaneously decreases for the furnace when expanding the valve opening ratio. It is worth noting that the particles are quite very scarce in the top FBHE, leading to the very little mass flow rate of particles from FBHE to the furnace. This could be caused by the underevaluated drag coefficient for FBHE, which is now based on operating parameters for the furnace. Because the furnace flow operates in a fast fluidization

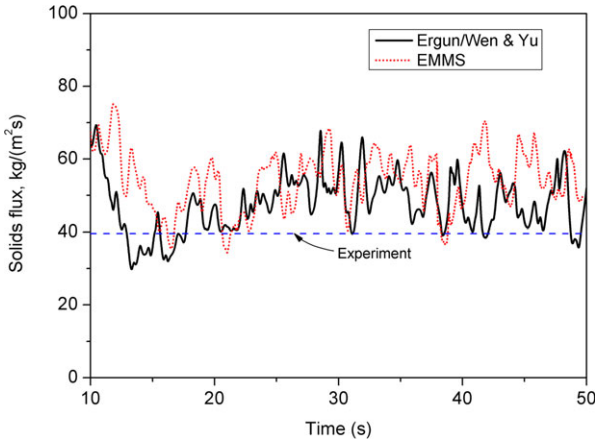

Figure 9. Comparison of circulating solids flux (based on the cross-sectional area of the upper furnace) using Ergun/Wen and Yu model and EMMS-based model.

[Color figure can be viewed in the online issue, which is available at wileyonlinelibrary.com.]

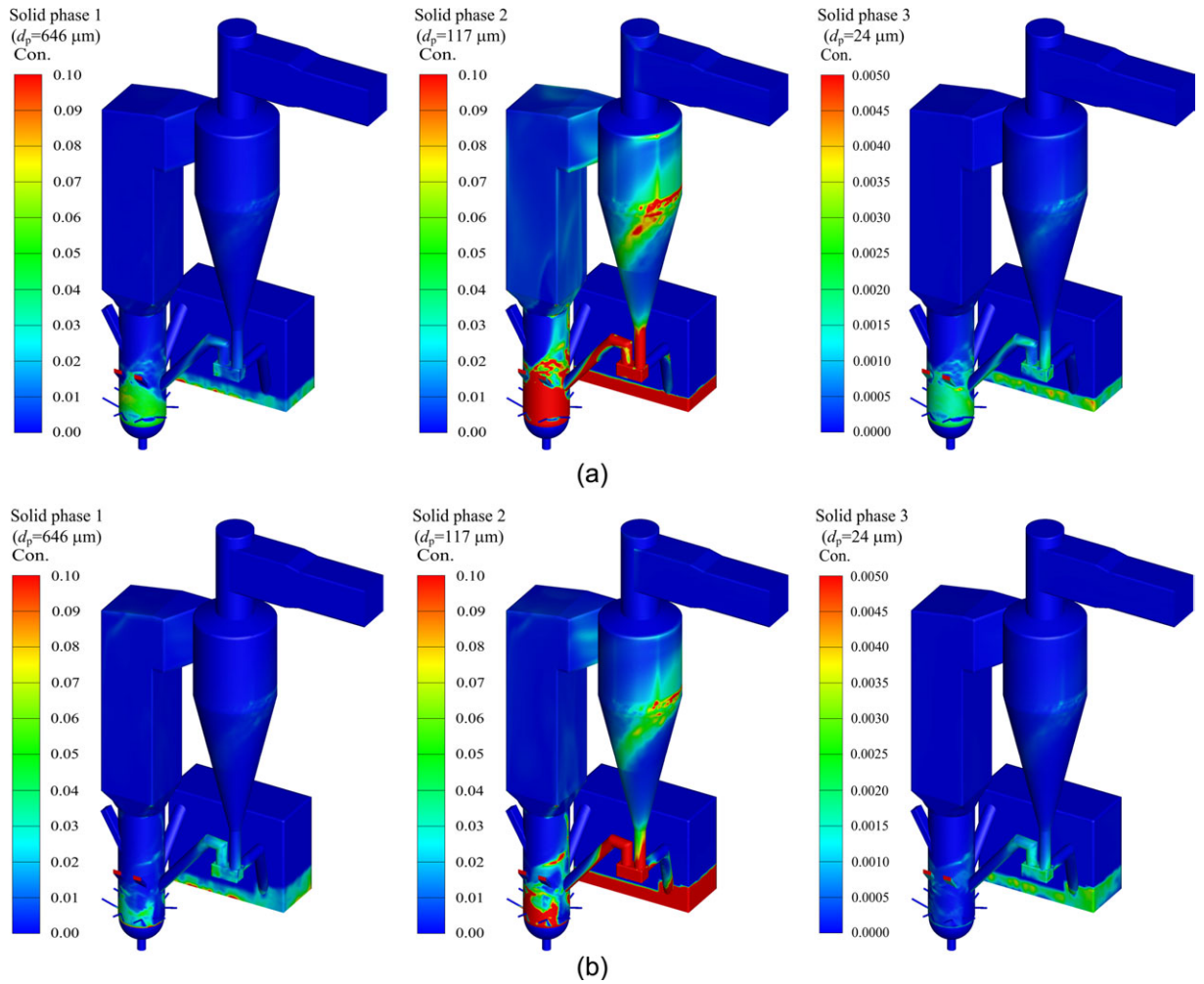

Figure 10. Snapshots of solids volume fraction (the solids concentration greater than 0.05 and 0.001 for the solid phases 1 and 2, and solid phase 3, respectively, is also denoted in red color): (a) with valve opening ratio of 1.5625%; (b) with valve opening ratio of 25%.

[Color figure can be viewed in the online issue, which is available at wileyonlinelibrary.com.]

regime where the particles generally move in the form of clusters, the corresponding drag coefficient is reduced significantly compared to that for the homogeneous state. However, FBHE flow runs in near bubbly or turbulent flow regime, showing more homogeneous flow structures compared to the fast fluidization. Therefore, the dependence of this drag coefficient on a single set of operating parameters may be modified to match with such a full-loop system where multiple subsections have variable flow states. Those relevant studies are under way.

After a period of computation, the ratio of each solid phase in different parts of the boiler experiences a change. Table 5 lists the ratio of each solid phase in the furnace, the cyclone and FBHE. Compared to the original situation, the ratio of large particles (S1) increases greatly for the furnace, and the second large particles (S2) and small particles (S3) are found to increase in the cyclone.

For the valve with larger opening ratio, the second large particles (S2) in the furnace are reduced greatly compared to that for the valve with a smaller opening. This implies that those particles are more likely to move into FBHE and little of those are returned into the furnace. Therefore, to maintain the high-circulating solids flow rate, particles in FBHE should be entrained high enough to enter the furnace.

Pressure distribution

Figure 11 compares the pressure along the central line of the whole boiler for both simulations. When the opening

Table 5. Mass Ratio of Each Solids Phase in the Furnace, the Cyclone and FBHE

		Mass ratio (furnace, %)		Mass ratio (cyclone, %)		Mass ratio (FBHE, %)	
Particle phase	Original ratio (%)	Valve 1 (1.5625%)	Valve 2 (25%)	Valve 1 (1.5625%)	Valve 2 (25%)	Valve 1 (1.5625%)	Valve 2 (25%)
S1 (d_p = 646 μm)	6.73	8.24	11.77	3.68	5.16	6.60	6.15
S2 (d_p = 117 μm)	92.66	91.17	87.58	95.23	93.58	92.82	93.28
S3 (d_p = 24 μm)	0.61	0.59	0.65	1.09	1.26	0.58	0.57

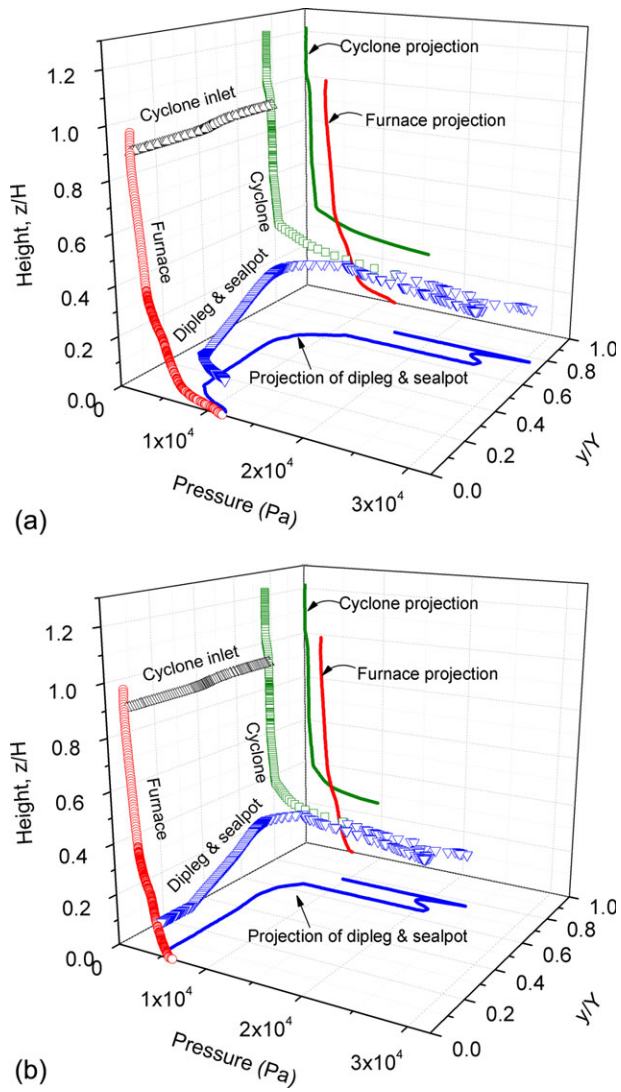

Figure 11. Simulated pressure balance in the full boiler ("0" in the *z*-direction is the position of the distributor above the plenum).

H is the total height of the furnace. *Y* is the distance between the centers of the furnace and the cyclone. The pressure data were obtained from the center line of the furnace, cyclone inlet, cyclone, seal pot and dipleg): (a) with valve opening ratio of 1.5625%; (b) with valve opening ratio of 25%. [Color figure can be viewed in the online issue, which is available at wileyonlinelibrary.com.]

ratio of the valve increases from 1.5625 to 25%, it is found that the pressure drops for both the furnace and the cyclone are reduced significantly while the pressure in the seal pot correspondingly increases. This means that particles are more easily to move into FBHE with expanding the valve opening.

Summary

For the full-loop simulation of the boiler without FBHE, the EMMS-based model and Ergun/Wen and Yu model are evaluated. The former captures more heterogeneous structures, reasonable downward particle velocities near the wall and also predicts successfully the pressure profile of the furnace. For behaviors of polydisperse particles, the EMMS-based model shows the better mixing of particles with different sizes than the Ergun/Wen and Yu model. The relevant experiment is required to evaluate such predictions of both models in mixing behaviors. In addition, both models slightly over-predict the solid flux probably because of the oversimplification of particle-size distribution. The effect of polydispersity is suggested to be considered in our later simulation of coal combustion.

For the simulation of the boiler with FBHE using the EMMS-based model, the pressure drop for both the furnace and cyclone is reduced significantly when the opening ratio of the valve increases from 1.5625 to 25%. The flow in FBHE is not fluidized well enough. This is likely due to the underpredicted drag coefficient for FBHE. Probably, this EMMS-based drag model based on the single set of operating parameters needs improvement to fit for the full-loop system where multiple flow regimes are generally coexistent. The further relevant work is still under way.

Acknowledgments

This work is financially supported by Alstom Power, Inc., and also financially supported by the Natural Science Foundation of China under Grant No.21106157 and 21176240, MOST under Grant No. 2011DFA61360 and 2012CB215003, and the "Strategic Priority Research Program" of Chinese Academy of Sciences under Grant No. KGCX2-YW-222 and XDA07080202.

Notation

d_{ave} = average particle diameter based on the size distribution of the entire granulate mixture at in the whole bed, m
$d_{ave,h}$ = average particle diameter based on the size distribution of the entire granulate mixture at a given elevation, m
d_p = particle diameter, m
G_s = solids flux, kg/m^2·s
H = total height of furnace, m
H_D = heterogeneity index
Re_s = Reynolds number, $d_p U_{slip} \rho_f / \mu_f$
U_g = superficial gas rate, m/s
$\boldsymbol{v}$ = real velocity, m/s

Greek letters

β = drag coefficient with structure in a control volume, kg/m^3 s
β_0 = drag coefficient without structure in a control volume, kg/m^3 s
ε_g = voidage
ε_s = solids concentration
ε_{mf} = incipient voidage
ε_{max} = maximum voidage for particle aggregation
μ = viscosity, Pa·s
σ = mixing index

Subscripts

g = gas phase
s = solid phase
p = particle

(Bold characters are for vectors or tensors)

Literature Cited

1. Ibsen CH, Helland E, Hjertager BH, Solberg T, Tadrist L, Occelli R. Comparison of multifluid and discrete particle modelling in numerical predictions of gas particle flow in circulating fluidised beds. *Powder Technol*. 2004;149:29–41.
2. Basu P, Sett A, Gbordzoe EAM. *A simplified model for combustion of carbon in a circulating fluidized bed combustor*. In: Mustonen J, ed. *Proceedings of the 9th International Conference on Fluidized Bed Combustion*. New York: ASME; 1987;738–742.
3. Huilin L, Guangbo Z, Rushan B, Yongjin C, Gidaspow D. A coal combustion model for circulating fluidized bed boilers. *Fuel*. 2000;79:165–172.

4. Adanez J, Gayan P, Grasa G, de Diego LF, Armesto L, Cabanillas A. Circulating fluidized bed combustion in the turbulent regime: modeling of carbon combustion efficiency and sulfur retention. *Fuel*. 2001;80:1405–1414.
5. Nikolopoulos A, Rampidis I, Nikolopouos N, Grammelis P, Kakaras E. *Numerical investigation of 3-D transient combusting flow in a 1.2MWTH pilot power plant*. In: Yue GX, Zhang H, Zhao CS, Luo ZY, eds. *Proceedings of the 20th International Conference on Fluidized Bed Combustion*, Xi'an, China: Springer; 2009;839–844.
6. Zhou W, Zhao CS, Duan LB, Qu CR, Chen XP. Two-dimensional computational fluid dynamics simulation of coal combustion in a circulating fluidized bed combustor. *Chem Eng J*. 2011;166: 306–314.
7. Zhang N, Lu B, Wang W, Li J. Virtual experimentation through 3D full-loop simulation of a circulating fluidized bed. *Particuology*. 2008;6:529–539.
8. Zhang N, Lu B, Wang W, Li J. 3D CFD simulation of hydrodynamics of a 150 MW_e circulating fluidized bed boiler. *Chem Eng J*. 2010;162:821–828.
9. Lu B, Wang W, Li J. Searching for a mesh-independent sub-grid model for CFD simulation of gas-solid riser flows. *Chem Eng Sci*. 2009;64:3437–3447.
10. Li J, Chen A, Yan Z, Xu G, Zhang X. *Particle-fluid contacting in circulating fluidized beds*. In: Avidan AA, ed. *Preprint Volume for Circulating Fluidized Beds IV*. Somerset: AIChE; 1993;49–54.
11. O'Brien TJ, Syamlal M. *Particle cluster effects in the numerical simulation of a circulating fluidized bed*. In: Avidan AA, ed. *Preprint Volume for Circulating Fluidized Beds IV*. Somerset: AICHE; 1993;345–350.
12. Sundaresan S. Modeling the hydrodynamics of multiphase flow reactors: current status and challenges. *AIChE J*. 2000;46:1102–1105.
13. Agrawal K, Loezos PN, Syamlal M, Sundaresan S. The role of mesoscale structures in rapid gas-solid flows. *J Fluid Mech*. 2001; 445:151–185.
14. Hartge EU, Ratschow L, Wischnewski R, Werther J. CFD-simulation of a circulating fluidized bed riser. *Particuology*. 2009;7:283–296.
15. Benyahia S. Analysis of model parameters affecting the pressure profile in a circulating fluidized bed. *AIChE J*. 2012;58:427–439.
16. Igci Y, Andrews IV AT, Sundaresan S, Pannala S, O'Brien T. Filtered two-fluid models for fluidized gas-particle suspensions. *AIChE J*. 2008;54:1431–1448.
17. Yang N, Wang W, Ge W, Li J. CFD simulation of concurrent-up gas-solid flow in circulating fluidized beds with structure-dependent drag coefficient. *Chem Eng J*. 2003;96:71–80.
18. Gidaspow D. Hydrodynamics of fluidization and heat transfer: supercomputer modeling. *Appl Mech Rev*. 1986;39:1–23.
19. Wang W, Li J. Simulation of gas-solid two-phase flow by a multi-scale CFD approach-extension of EMMS model to the sub-grid level. *Chem Eng Sci*. 2007;62:208–231.
20. Lu B, Wang W, Li J. Eulerian simulation of gas-solid flows with particles of Geldart groups A, B and D using EMMS-based meso-scale model. *Chem Eng Sci*. 2011;66:4624–4635.
21. Couturier MF, Doucette B, Stevens D, Poolpol S, Razbin V. *Temperature, gas concentration and solid mass flux profiles within a large circulating fluidized bed combustor*. In: Anthony EJ, ed. *Proceedings of the 11th International Conference on Fluidized Bed Combustion*. Montreal, Canada: ASME; 1991;107–114.
22. Couturier MF, Steward FR, Poolpol S. *Experimental determination of heat transfer coefficients in a 72 MWT circulating fluidized bed boiler*. In: Lynn R, ed. *Proceedings of the 12th International Conference on Fluidized Bed Combustion*. San Diego, CA: ASME; 1993;1215–1222
23. Dahl SR, Hrenya CM. Size segregation in gas-solid fluidized beds with continuous size distributions. *Chem Eng Sci*. 2005;60:6658–6673.
24. Fan R, Fox RO. Segregation in polydisperse fluidized beds: Validation of a multi-fluid model. *Chem Eng Sci*. 2008;63:272–285.
25. Sofiane B. Verification and validation study of some polydisperse kinetic theories. *Chem Eng Sci*. 2008;63:5672–5680.
26. Holloway W, Benyahia S, Hrenya CM, Sundaresan S. Meso-scale structures of bidisperse mixtures of particles fluidized by a gas. *Chem Eng Sci*. 2011;66:4403–4420.
27. Hrenya CM. *Kinetic theory for granular materials: polydispersity*. In: Pannala S, Syamlal M, O'Brien TJ, ed. *Computational gas-solid flows and reacting systems: Theory, methods and practice. Kinetic theory of granular materials: polydispersity*. Hershey, PA: IGI Global; 2011;102–127
28. Beetstra R, van der Hoef MA, Kuiper JAM. Drag force of intermediate Reynolds number flow past mono- and bidisperse arrays of spheres. *AIChE J*. 2007;53:489–501.

Manuscript received Apr. 26, 2012, and revision received July 19, 2012.